Macromolecules
ARTICLE

*Macromolecules* **2010**, *43*, 6655–6665 **6655**
DOI: 10.1021/ma1002084

# Shear Deformation and Ferroelectricity in Chiral SmC* Main-chain Elastomers

**Patrick Heinze and Heino Finkelmann***

*Institut für Makromolekulare Chemie, Albert Ludwigs-Universität Freiburg, Stefan-Meier-Strasse 31, 79104 Freiburg im Breisgau, Germany*

*Received January 27, 2010; Revised Manuscript Received June 2, 2010*

ABSTRACT: Ferroelectric smectic main-chain liquid crystalline elastomers were synthesized and subjected to simple shear deformation to achieve reorientation of the layer structure and the formation of a macroscopic spontaneous polarization. The phase behavior and structural parameters of these elastomers are investigated and discussed. A shear-induced splitting of the X-ray scattering intensity distribution is found. A splitting of the sample in domains of two director orientations that couple differently to the shear deformation is proposed. The smectic layers also move at different affinities depending on their initial orientation. The smectic layer spacing was found to be nearly constant even though the smectic tilt angle changes significantly. The realignment of the smectic layers indicates a migration process, where depending on their original orientation the layer normals are leaving or entering the X-ray scattering plane. The spontaneous polarization was found to be linearly dependent on the dopant concentration with Ps = 30 nC/cm$^2$ for a system doped with 11 wt % of chiral dopant.

## Introduction

Liquid crystal elastomers (LCE) combine the elasticity of conventional rubbery networks with the anisotropic properties of crystalline materials. Depending on the molecular structure of the liquid crystal moieties, all mesomorphic structures that are found in low molar mass liquid crystals can be realized in such polymeric and elastomeric systems. Detailed reviews can be found in the literature.[1−3] Introduction of chirality to a SmC-phase leads to a nonzero polarization vector that points perpendicular to the plane that is spanned by the director and the smectic layer normal.[4−6] Because of the strong coupling between the liquid crystalline order and the polymer backbone, such systems show interesting new features such as piezoelectricity,[7,8] the generation of second harmonics,[9,10] and ferroelectric actuation through electric fields.[11,12]

Uniform orientation of the polarization vector leads to a high-energy state and consequently, in the absence of external fields, this polar vector is canceled out macroscopically by a helical superstructure of the SmC*-phase and all special properties of the SmC*-phase are lost.[13,14] Hence, a central problem pertains to the orientation of such systems.

Orientation and reorientation of the director of liquid crystalline elastomers has been investigated in detail. Electric and mechanical fields can be employed to achieve uniaxial director orientation.[15−17] Macroscopically uniaxial orientation of the director of a nematic liquid crystal yields what is called a liquid single crystal elastomer (LSCE). In smectic-A-elastomers, where the smectic layers are oriented perpendicular to the director, orientation of the director also results in a macroscopic orientation of the smectic layers.[18−21] In the case of the SmC-phase, both chiral and achiral, a uniaxial field is not sufficient anymore to obtain a liquid single crystal elastomer. In these liquid crystals, the smectic layer normal is not oriented parallel to the director but tilted by the angle $\theta$. As a field applied along the $z$-axis to orient the director leaves all orientations in the $x-y$-plane energetically degenerate, a conical distribution of the layer normals **k** around the director **n** will occur (see Figure 1). Because of the axis of improper reflection along the director, the vector of spontaneous polarization is canceled out on a macroscopic level.[9,10,22]

Macroscopic uniform orientation of the smectic layers can be achieved by a biaxial orientation process, where the director is uniaxially oriented in the first step, followed by the application of a second external field to achieve orientation of the layers. In the case of chiral smectic-C polymers and elastomers, alignment through electric fields is possible.[11] However, with saturation voltages in the range of 10 V/$\mu$m, this approach is limited to thin films. For thicker films above 50−100 $\mu$m the employment of a biaxial mechanical field seems more feasible. Several experimental conditions have been suggested in literature, where a uniaxial field is applied in various directions with respect to the director and the smectic layer orientation.[10,23] A well-examined method is to apply a simple shear perpendicular to the director of an uniaxially preoriented SmC-elastomer as suggested by Hiraoka et al. in 2001.[24,25]

In this paper, we report on the synthesis of a chiral smectic main-chain elastomer. The chirality is realized by doping a well-known SmC-system with a chiral comonomer. A homologous series of coelastomers with varying amounts of the chiral comonomer is investigated. The phase behavior and structural properties are analyzed. The elastomers are deformed by simple shear to achieve reorientation of the smectic layers. The reorientation process is monitored by X-ray diffraction studies as well as by measurement of the spontaneous polarization **Ps**.

## Experimental Section

**Synthesis of the Monomers.** For the synthesis of the chiral dopant **1** (see Scheme 1), chiral induction was achieved by enzymatically catalyzed[26] asymmetric addition of HCN to the aldehyde group of pent-1-en-5-al **2** which lead to the chiral cyanohydrine **3**. For the rigid core, *p*-hydroxycarboxylic methyl carboxylate **4** and

*Corresponding author. E-mail: Heino.Finkelmann@makro.uni-freiburg.de.

© 2010 American Chemical Society

Published on Web 07/26/2010

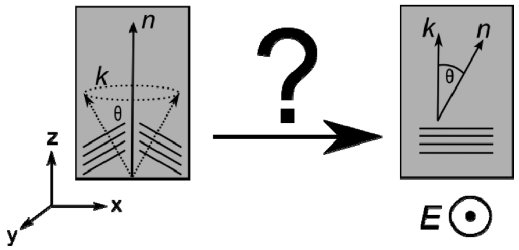


**Figure 1.** Left hand side: a SmC/SmC* *pseudo*-monodomain with a uniform director orientation, but conical distribution of layers, where **n**, **k**, and $\theta$ denote the director, layer normal, and smectic tilt angle, respectively. Right hand side: a SmC liquid single crystal with uniform director orientation and uniform layer orientation. Chiral samples in this orientation possess a macroscopic polarization vector (pointing along the *y*-direction) and show effects like second harmonic generation and, in the case of elastomers, piezoelectricity.

**Scheme 1. Synthesis of the Chiral Dopant 1**

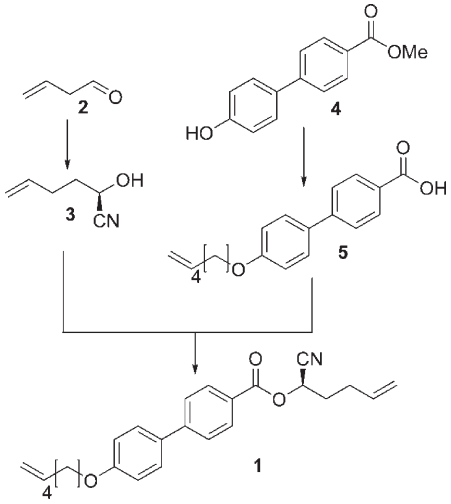


hex-1-en-6-ol were linked by a Mitsunobu etherification. After saponification of the methyl-protecting group, the chiral cyanohydrine **3** was coupled to the acid group of the rigid core **5** via a DCC-esterification to give the chiral dopant **1**. The synthesis of the smectic host monomer **6** is described in literature.[27]

**(*R*)-2-Hydroxy-hex-5-ennitrile (3).** Almond meal (200 g) was stirred in diethyl ether (800 mL) overnight. The suspension was centrifuged and the almond meal was dried *in vacuo*. The dry meal was stirred in citric acid buffer (500 mL, pH = 3.3, 25 mM) overnight. Centrifugation gave a clear yellow enzymatic solution. Phosphoric acid (85%, 7.5 mL) and diethyl ether (100 mL) were placed into a separating funnel. An ice-cooled solution of sodium cyanide (256 g, 52 mmol) in water (20 mL, 0 °C) was added (Caution! formation of highly toxic gases). The funnel was shaken and the organic layer was separated. Commercially available pent-1-en-5-al (**2**) (2.00 g, 24 mmol) in diethyl ether (25 mL) was added to the enzymatic solution (100 mL) and stirred. The HCN-containing ethereal solution was added dropwise over 1 h and the reaction mixture was stirred for a further 2 h. The reaction mixture was extracted with diethyl ether (4 × 100 mL). The combined ethereal phases were dried over $MgSO_4$ and concentrated *in vacuo*. Distillation (1.5 mbar, 67 °C) gave (*R*)-2-hydroxy-hex-5-ennitrile (**3**) as a colorless oil (2 g, 76%). $[\alpha_d^{20}]$ = 8.12° in $CHCl_3$, $^1$H NMR (300.13 MHz, $CDCl_3$), $\delta$ [ppm]: 5.72−5.86 (m, 1H), 5.08 (t, 2H), 4.48 (t, 1H), 2.23−2.31 (m, 2H), 1.90−2.02 (m, 2H), $^{13}$C NMR (75.47 MHz, $CDCl_3$), $\delta$ [ppm]: 135.92, 119.87, 116.60, 60.49, 34.01, 28.59

**4′-(Hex-5-en-1-yloxy)biphenyl-4-carboxylic Acid (5).** Triphenylphosphine ($PPh_3$, 3.5 g, 13.3 mmol) and 4′-(hydroxy)biphenyl-4-methylcarboxylate (**4**) (2.9 g, 12.7 mmol) were dissolved in dry THF (100 mL) and purged with dry argon for 30 min. The solution was cooled to 0 °C and hex-1-en-6-ol (1.34 g, 13.3 mmol, commercially available in 99%) was added. Diisopropylazodicarboxylate (DiPAD, 2.7 g, 13.3 mmol) was dissolved in dry THF (20 mL) and added to the reaction mixure dropwise. The mixture was then stirred overnight at ambient temperature. The solvent was evaporated and the solid residue was extracted with ethyl acetate (40 mL). The remaining residue (crude intermediate product, free from $PPh_3O$) was put aside. The ethyl acetate was mixed with isohexane (200 mL) and the white precipitate ($PPh_3O$) was filtered. The filtrate and the crude intermediate product were combined and concentrated *in vacuo*, partially dissolved in methanol (250 mL) and aquaeous NaOH-solution (2.5 g, 64 mmol in 25 mL water) was added. The mixture was stirred at reflux temperature for 2 h. The solvent was evaporated off and the solid residue was partially dissolved in water (500 mL). After cooling to 0 °C, HCl (10 mL) was added until a pH of 1 was reached. The precipitate was filtered and washed with water until neutral. Recrystallization from ethanol/water 70:30 gave the title compound **5** as white crystals (3.08 g, 82%). $^1$H NMR (300.13 MHz, $CDCl_3$), $\delta$ [ppm]: 7.95 (d, 2H), 7.63 (d, 2H), 7.55 (d, 2H), 6.92 (d, 2H), 5.80−5.66 (m, 1H), 4.86 (dd, 2H), 3.95 (t, 2H), 2.02 (dt, 2H), 1.70 (tt, 2H), 1.47 (tt, 2H).

**(*R*)-1-Cyanopent-4-en-1-yl 4′-(Hex-5-en-1-yloxy)biphenyl-4-carboxylate (1).** Dimethylaminopyridine (DMAP, 0.41 g, 3.37 mmol) and 4′-(hex-5-en-1-yloxy)biphenyl-4-carboxylic acid (**5**) (1.0 g, 3.37 mmol) were dissolved in dry $CH_2Cl_2$ (40 mL) and dry THF (20 mL). A solution of dicyclohexylcarbodiimide (DCC, 0.70 g, 3.37 mmol) in $CH_2Cl_2$ (20 mL) was added, followed by addition of a solution of (*R*)-2-hydroxy-hex-5-ennitrile (**3**) in $CH_2Cl_2$ (20 mL). The solution was then stirred overnight at ambient temperature. The white precipitate was filtered and discarded, and the filtrate was concentrated *in vacuo*. Flash column chromatography (silica, isohexane/ethyl acetate) followed by recrystallization from methanol/water 7:3 and freeze-drying from benzene gave the desired compound as white crystals (1.16 g, 89%). $[\alpha_d^{20}]$ = 9.87° in $CHCl_3$, $^1$H NMR (300.13 MHz, $CDCl_3$), $\delta$ [ppm]: 8.09 (d, 2H), 7.65 (d, 2H), 7.57 (d, 2H), 7.00 (d, 2H), 5.62−5.91 (m, 2H), 5.62 (t, 1H), 4.97−5.18 (m, 4H), 4.03 (t, 2H), 2.34 (dt, 2H), 2.11−2.22 (m, 4H), 1.84 (tt, 2H), 1.61 (tt, 2H).

**4-Hex-5-en-1-yloxy)phenyl 4-(Hex-5-en-1-yloxy)benzoate (6).** The synthesis of 4-(hex-5-en-1-yloxy)phenyl 4-(hex-5-en-1-yloxy)-benzoate is described in the literature.[27]

**Synthesis of the elastomers.** Elastomers with compositions as shown in Table 1 were synthesized in a spin-casting cell by a platinum catalyzed hydrosilylation step-growth reaction using toluene as solvent. 2,4,6,8,10-Pentamethylcyclopentasiloxane **7** and 1,1,3,3-tetramethyldisiloxane **8** were used as crosslinker and chain-extender, repectively. The samples were oriented uniaxially by application of a nominal stress of 45 ± 5 kPa with respect to the dimensions at room temperature. The orientation was fixed by a second cross-linking step,[17] where the elastomers were kept in the SmC-phase at 50 °C for 1 week. All elastomers were extracted with toluene, soluble fractions were found to be around 13% ± 1% for all elastomers. Sample thickness was generally 350 ± 20 $\mu$m.

**X-ray Measurements.** The measurements were performed using a custom-made SAXS/WAXS setup by JJ X-ray Systems consisting of a Rigaku Micromax-002+ Micro focus X-ray source and a Bruker AXS Hi-Star detector with a resolution of 1024 × 1024 pixels. The sample was placed in a self-constructed sample holder where temperature control was achieved by a Eurotherm

**Table 1. Composition of the Synthesized Elastomers**

| | dopant **1** [mg] | host **6** [mg] | cross-linker **7** [mg] | siloxane **8** [mg] | dopant fraction [wt %] |
|---|---|---|---|---|---|
| E0 | 0 | 634.4 | 23.8 | 189.4 | 0 |
| E4 | 31.9 | 599.9 | 24.1 | 188.4 | 3.8 |
| E7 | 62.3 | 573.5 | 24.3 | 188.6 | 7.3 |
| E11 | 93.5 | 536.5 | 24.0 | 188.1 | 11.1 |
| E15 | 125.3 | 504.8 | 24.0 | 188.3 | 14.9 |

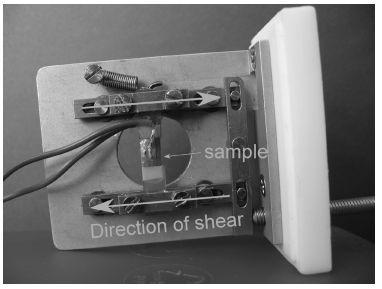


**Figure 2.** Photograph of the shear apparatus and electrically contacted sample. Simple shear can be induced by turning the screw on the lower right side of the picture. Electrically conducting silver grease was spread on the elastomer and great care was taken not to short-circuit the two faces.

3216 PID-controller where the temperature was ±0.5 K. The distance between sample and detector (calibrated by using silver behenate as a standard) was 1683 mm for the measurements of smectic layer spacings. For the wide-angle and shear-dependent measurements, the distance between sample and detector was 250 mm, which allowed simultaneous detection of the wide-angle and the small-angle peaks.

High-resolution SAXS-pictures under shear were taken on BW4 at the HASYLAB synchrotron facility in Hamburg, Germany. The wavelength of the incident beam was $\lambda = 0.13808$ nm, for detection a marCCD165-Detector with a resolution of 2048 · 2048 pixels was used. Distance between sample and detector was 1313 mm, Lupolene and silver behenate were used as standards. For temperature control, the same setup as in the experiments using the JJ X-ray system was used.

For the shear measurements, the sample was glued on aluminum plates by 2-component epoxy glue. The plates were clamped to a self-constructed shear apparatus that allows the induction of a simple shear (Figure 2). The shear is induced by manually turning a screw, which in turn presses against the slider rails. A photograph of the sample was taken every four shear steps, from which the induced shear angle $\beta$ was determined. The interjacent angles were determined by linear interpolation. All experiments were conducted at $T_{red} = T/T_{SI} = 0.944$ which corresponds to 46 °C for E15 and 55 °C for E0. $T_{SI}$ is the temperature at which the transformation from the smectic to the isotropic phase takes place. At this reduced temperature, all elastomers are sufficiently below the isotropization temperature and still far away from $T_g$ so as to omit any possible artifacts due to nonequilibrium conditions. To allow for relaxation, waiting time between consecutive shear steps was 20 min. Sample dimensions in $x$- and $z$-directions were around $5 \times 6$ mm$^2$ in all shearing experiments.

**Measurement of the Spontaneous Polarization.** Sample preparation, aspect ratios and temperatures were the same as in the X-ray experiments. Between consecutive shear steps there was a gap of 20 min. Electrically insulating Pertinax plates were used for clamping rather than aluminum. Silver conductive grease was spread on both sides of the sample surface, which was connected to a Kistler 5011 charge amplifier. The area of the electrodes was $5 \times 6$ mm$^2$. All parts of the experiment, including temperature cell and shear apparatus, were carefully grounded to the charge amplifier's ground. In these quasi-static experiments, a long time constant (>10 000 s), and a low-pass filter of 10 Hz was used. Transducer sensitivity was 10 pC/mechanical unit and scale was 100 mechanical units/V, resulting in an effective resolution of 1 nC/V. The ±10 V signal of the charge amplifier was measured with a Tektronix TDS 3032B digital oscilloscope.

**DSC.** DSC measurements were carried out using a PerkinElmer DSC-7 at heating rates of 9, 16, 26, and 36 K/min. Glass transition and phase transformation temperatures were determined by extrapolating to a heating rate of 0 K/min. The experimental error for the phase transformation temperatures is estimated to be ±1 °C and ±5 °C for $T_g$. Experimental error for phase transition enthalpies and $\Delta c_p$ is estimated to be ±0.5 J/g and ±0.05 J/g, respectively.

**Scheme 2. Synthesis of the Liquid Crystalline Elastomers (LCE) via a Platinum-Catalyzed Step-Growth Polyaddition Reaction**

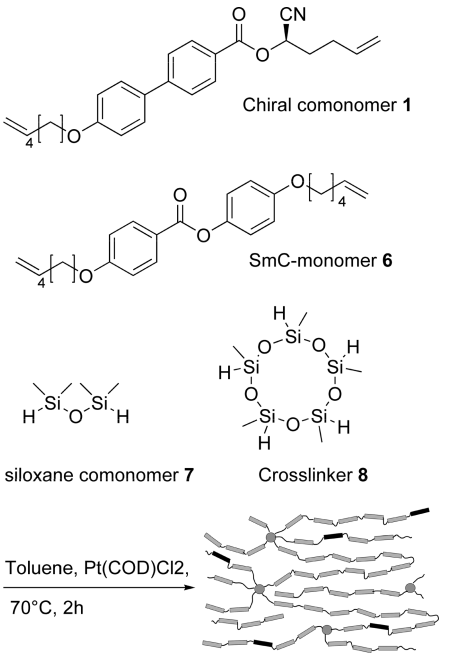


## Results and Discussion

The aim of this investigation is to follow the reorientation process of a uniaxially preoriented SmC* main-chain LCE by means of X-ray diffraction and by measurement of the spontaneous polarization. For this, a chiral smectic main-chain LCE has been synthesized, where the chirality is achieved by doping a SmC-host-system. A homologous series of chiral coelastomers is investigated to learn more about the influence of the chiral comonomer **1** on the phase behavior and the ferroelectric and structural properties of the system.

Chiral smectic main-chain LCE were synthesized via the well-known 2-step procedure, where the weakly cross-linked sample is oriented uniaxially and the order is fixed by a second cross-linking step under uniaxial load (Scheme 2).[17,27] This leads to samples with a stable macroscopic orientation of the director while the smectic layers are distributed conically around the director (see the left side of Figure 1). The chiral comonomer **1** has been designed with the aim of producing high spontaneous polarizations $\mathbf{P_s}$. It closely resembles a well-known low molar mass compound which is reported to produce high values of $\mathbf{P_s}$ at low dopant fractions.[28] The high $\mathbf{P_s}$ is caused by the strongly polar nitrile group which is located near the aromatic system of the biphenyl core of **1**.[5] However, both the chiral comonomer **1** used here and the corresponding low molar mass compound are not intrinsically liquid crystalline and have to be mixed with the smectic C host monomer. With the chemistry employed here, the chiral dopant **1** is chemically attached to the liquid crystalline network during the elastomer synthesis. Elastomers **E0**, **E4**, **E7**, **E11**, and **E15** with 0, 4, 7, 11, and 15 wt %, respectively, of chiral comonomer **1** were synthesized.

All elastomers exhibit a broad SmC*-phase (SmC in the case of the nondoped elastomer). Their isotropization temperature $T_{SI}$ decreases from 76 °C in the case of the nondoped elastomer **E0** to 65 °C in the case of **E15** with 15 wt % chiral dopant **1** content (see Table 2). A tilted smectic phase of higher order that occurs at $T_{SH}$ below room temperature in the nondoped elastomer **E0** is gradually suppressed with increasing dopant content and is not exhibited in **E15**. The $T_g$ decreases with increasing amounts of

chiral comonomer and is in the range of 0 °C. No $T_g$ is found for the nondoped elastomer **E0** in DSC-measurements. Presumably, the change of heat capacity $\Delta c_p$ at $T_g$ is too low to be detected when the already highly immobilized chains undergo glassy freezing in the hexagonally ordered smectic phase.

Table 3 shows the structural data of **E0**, **E4**, **E7**, **E11**, and **E15** as determined by small-angle X-ray diffraction. The order parameter $S$ was measured by evaluation azimutal scattering intensity distribution of the of the wide-angle regime.[29,30] $S$ remains constant for all the elastomers. With increasing content of chiral dopant **1**, the tilt angle $\theta$ between the director **n** and the smectic layer normal **k** decreases. Simultaneously, the smectic interlayer spacing $d$ increases. This could be explained by the biphenyl units of **1**. Biphenyl containing mesogens are known to induce SmA-phases in main-chain polymers.[12,31,32] Thus, increasing amounts of the biphenyl-core of the chiral dopant also causes lower tilt-angles.

**Table 2. Phase Behavior of the Synthesized Elastomers As Determined by DSC**

| | $T_{SI}$ [°C] | $\Delta H_{SI}$ [J·g$^{-1}$] | $T_{SH}$ [°C] | $\Delta H_{SH}$ [J·g$^{-1}$] | $T_g$ [°C] | $\Delta c_p$ [K·J g$^{-1}$] |
|---|---|---|---|---|---|---|
| E0 | 76 | 10.7 | 25 | 4.9 | | |
| E4 | 72 | 10.4 | 16 | 4.3 | 2 | 0.32 |
| E7 | 69 | 10.3 | 5 | | −2 | 0.39 |
| E11 | 69 | 10.1 | 5 | | −3 | 0.32 |
| E15 | 65 | 9.8 | | | −4 | 0.34 |

**Table 3. Order parameter $S$, Smectic Tilt Angle $\theta$, Smectic Interlayer Spacing $d$, Calculated Mean Length of the Mesogens $l_m$ and Fraction $\mu$ of Lorentzian and Gaussian Line Shape of the Azimuthal Small Angle Distribution of the Elastomers E0, E4, E7, E11, and E15 at $T_{red}$ = 0.944 As Determined by X-ray Scattering**

| | $S$ | $\theta$ [deg] | $d$ [Å] | $l_m$ [Å] | $\mu$ |
|---|---|---|---|---|---|
| E0 | 0.78 ± 0.01 | 30.5 ± 0.3 | 26.2 ± 0.1 | 30.3 ± 0.2 | 0.6 ± 0.1 |
| E4 | 0.78 | 29.0 | 26.3 | 29.9 | 0.6 |
| E7 | 0.79 | 281 | 26.5 | 29.9 | 0.7 |
| E11 | 0.79 | 26.6 | 26.6 | 29.6 | 0.7 |
| E15 | 0.79 | 26.1 | 26.8 | 29.7 | 0.6 |

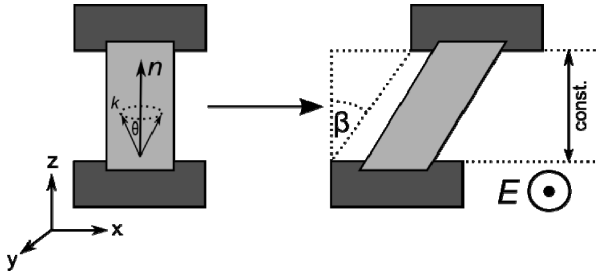


**Figure 3.** Schematic of the shear deformation geometry together with a definition of the shear angle $\beta$ and the coordinate system of the experiment.

To determine if an increasing amount of **1** also affects the smectic interlayer spacing, a mean length $l_m$ of the mesogens was calculated from the measured values of $\theta$ and $d$ by

$$l_m = \frac{d}{\cos\theta} \tag{1}$$

The length $l_m$ calculated this way does not represent the length of an actual mesogen. Rather, $l_m$ represents a hypothetical length of the mixture of the chiral dopant and the SmC-host-phase as it is seen in X-ray diffraction. The values of $l_m$ are also listed in Table 3. The computed length of the all-trans configuration in vacuum of the polymer repeating units of the chiral dopant **1** is 30 and 33 Å for the host **6**. Since **1** is about 10% shorter than **6**, a decrease of $l_m$ was expected at higher fractions of chiral dopant. However, the $l_m$ found in these elastomers is constant within experimental error. The length $l_m$ found by eq 1 is a few Å smaller than the computed length of both molecules. This is most likely an effect of the median inclination of the mesogens' long axis caused by the order parameter $S < 1$, which reduces the effective length of the mesogens in the $z$-direction.[33]

When fitting the azimuthal distribution of the small-angle regime with a *pseudo*-Voigt linear combination of a Lorentzian and Gaussian, where $\mu$ is the linear combination parameter ($\mu = 1$ for a pure Lorentzian line shape and $\mu = 1$ for a pure Gaussian), we find that all the samples exhibit values of $\mu \approx 0.6 \pm 0.1$. Thus, the azimuthal distribution of layers in these samples is more Lorentzian than Gaussian. When using the same fitting function for the azimutal wide-angle distribution, we find a pure Gaussian distribution with $\mu \approx 0$ in all samples.

**Shear Deformation.** In order to investigate the reorientation process under shear, X-ray scattering images of the sample were taken at different shear angles. A schematic of the shear setup, together with a definition of the shear angle $\beta$ and the coordinate system, is shown in Figure 3. The sample is oriented with the director along the $z$-direction. The shear is applied in the $xz$-plane by moving the clamping plates perpendicular to the director along the $x$-axis. The incident beam was directed along the $y$-axis. The shear setup is similar to the one used by Sánchez-Ferrer[24] and Hiraoka.[25] However, an important difference is that the sliding rails in this setup move parallel throughout the whole shear process to ensure a simple shear in contrast to the tilting and thereby compressing movement used in the mentioned works. In the following section, the shear process is discussed for the elastomer **E7** with 7 wt % of chiral dopant at 50 °C, which corresponds to a reduced temperature of $T_{red} = T/T_{SI} \approx 0.944$. The other elastomers with different amounts of chiral dopant behave essentially similar.

Figure 4 shows the X-ray diffraction patterns at shear angles of 0, 16, 27 and 38°. The diffuse outer peaks represent the lateral spacing of the mesogens similar to the X-ray diffraction pattern of a nematic liquid crystal and are oriented perpendicular to the director. The broad azimuthal

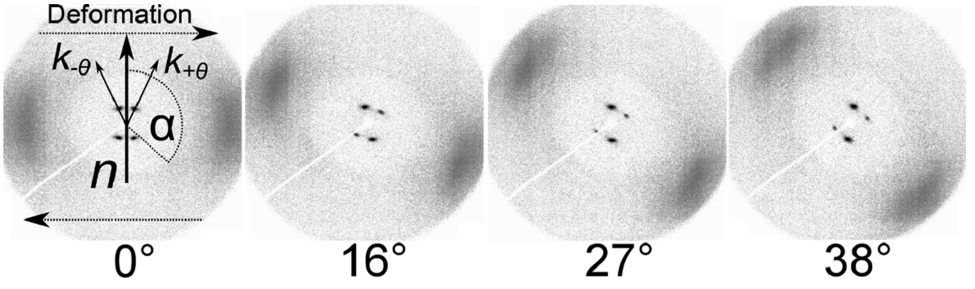


**Figure 4.** X-ray diffraction patterns for E7 at various shear angles at $T_{red} = 0.944$. Even at high shear angles, no perfect monodomain is formed. In the left picture, the direction of deformation and director orientation are depicted and the azimuthal angle α and the layer normals $\mathbf{k}_{-\theta}$ and $\mathbf{k}_{+\theta}$ are defined.

intensity distribution is a measure of the orientational disorder which can be quantified by the nematic order parameter $S$.[29,30] At zero shear, the director $\mathbf{n}$ is oriented along the $z$-direction of the scattering image. The small-angle peaks are denoting a positional preference of the mesogens center of gravity as they arrange in the smectic layers.[14] The smectic layer normal $\mathbf{k}$ is oriented along the small angle peaks (Figure 1). The conical distribution of the layer normals is reflected in the splitting into 4 peaks with layer normals $\mathbf{k}_{-\theta}$ and $\mathbf{k}_{+\theta}$ . In the scattering experiment, only the layers with the layer normal in the $x-z$-plane contribute to the scattering process and only these layers are detected. Because the symmetry axis runs along the director, turning the sample around the $z$-direction will yield identical scattering images at all angles. Figure 4 shows that shear deformation leads to a rotation of the wide- and small-angle peaks. Thus, both the director and the smectic layers are coupling to the shear deformation and are rotating accordingly. Also, the SAXS-peaks that correspond to the layer normal $\mathbf{k}_{+\theta}$ are gradually losing intensity while the pair of the layer normal $\mathbf{k}_{-\theta}$ become more intense. However, even for high shear angles, the peaks of the layer normal $\mathbf{k}_{+\theta}$ do not disappear completely. This is contradictory to previous reports.[24,25]

In the next section, the shear process will be investigated in detail for both the small- and the wide-angle regime.

**Wide-Angle Regime.** To analyze the rotation of the director, scans of the scattering intensity as a function of the azimuthal angle α were taken (see Figure 4 for a definition of α). The azimutal scattering distribution is a macroscopic representation of the microscopic orientational distribution function of the director. In the uniaxially oriented liquid crystal elastomer in unsheared state, a uniform Gaussian distribution is found where the maximum represents the mean orientation of the mesogens long axis. This mean orientation can be interpreted as the orientation of the macroscopic director. Therefore, by determination of the peak maximum of the scattering distribution, the azimutal orientation of the director can be extracted. With increasing shear the wide-angle peak transforms more and more into a Lorentzian line shape. This can be quantified by fitting the azimutal distribution with a *pseudo*-Voigt function. This fitting process yields reasonable results up to shear angles of roughly $\beta \approx 25°$. At higher shear angles, the intensity distribution profile cannot be represented by a single fitting function anymore. Instead, a linear combination of two separate peak functions has to be used. Such a model represents the intensity distribution very closely. The standard deviation of the fitting parameters is as low as in the "normal" fitting process of the unsheared sample with a single Gaussian peak function. We therefore believe that the model comprising two peak functions is statistically reliable.

As the peak maximum of the scattering distribution denotes the orientation of the director, the process that is observed here can be interpreted as a shear induced splitting of the sample into domains of two different director orientations. It therefore seems, that at high shear angles, we do not have to consider only one director, but a trailing director $\mathbf{n}_-$ at lower azimuthal angles and a leading director $\mathbf{n}_+$ at higher azimuthal angles (Figure 5). Such a process has not yet been reported in literature and seems to be a direct result of the shear process. At medium shear angles, around 25°, where the peak splits into two, both fitting methods will give imprecise results. It seems reasonable to analyze the rotation of the director by using the *pseudo*-Voigt profile at low shear angles and the multiple-peak function at high shear angles.

Several functions can be used for the linear combination to fit the wide-angle scattering distribution after the splitting process. Before the start of the splitting process, the intensity

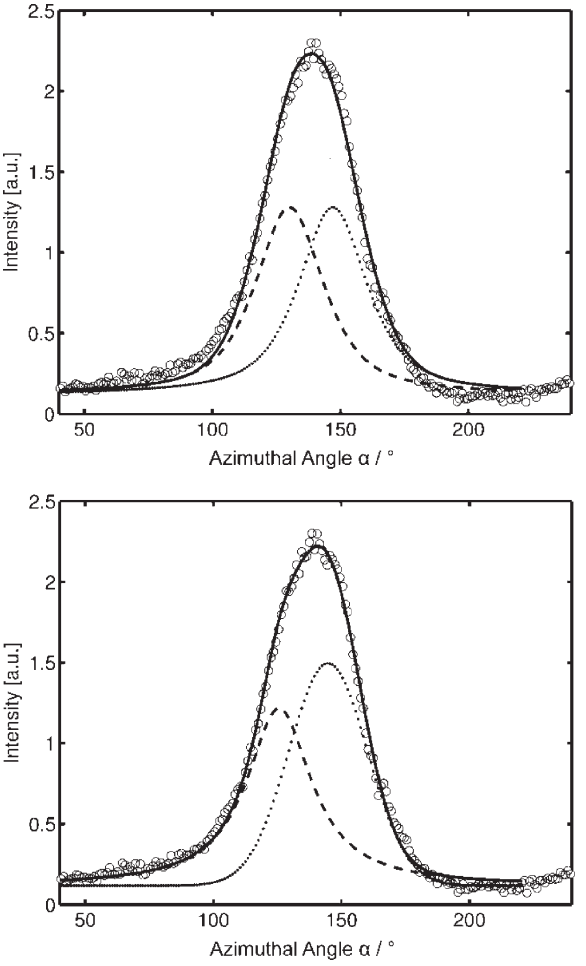


**Figure 5.** Separation of the wide-angle intensity distribution into several components at shear angle $\beta = 40°$. Upper plot: Superposition of two *pseudo*-Voigt functions with $\mu = 0.8$. Lower plot: Superposition of a Gaussian distribution (dotted line) and a Lorentzian distribution (dashed line).

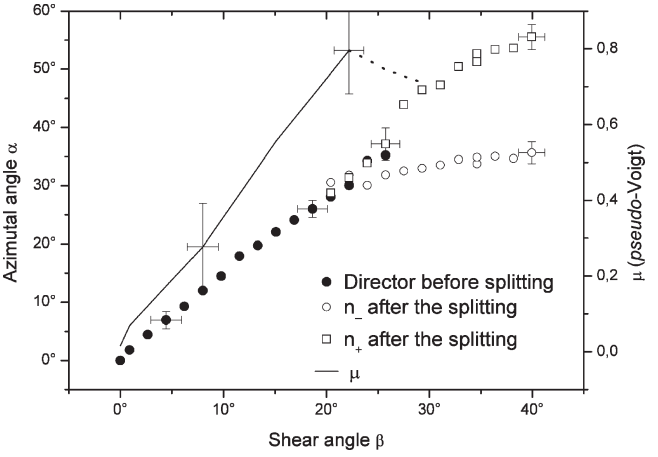


**Figure 6.** Angular rotation of the director and splitting into two populations ($T_{red} = 0.944$). The gray line depicts the $\mu$-value of the *pseudo*-Voigt function, that is, the Lorentzian fraction in the wide-angle peak before the splitting occurs.

distribution profile could be described by a *pseudo*-Voigt peak function with $\mu = 0.8$. It seems reasonable to assume that after the splitting the two separate peaks remain in such peak forms. However, this superposition does not represent

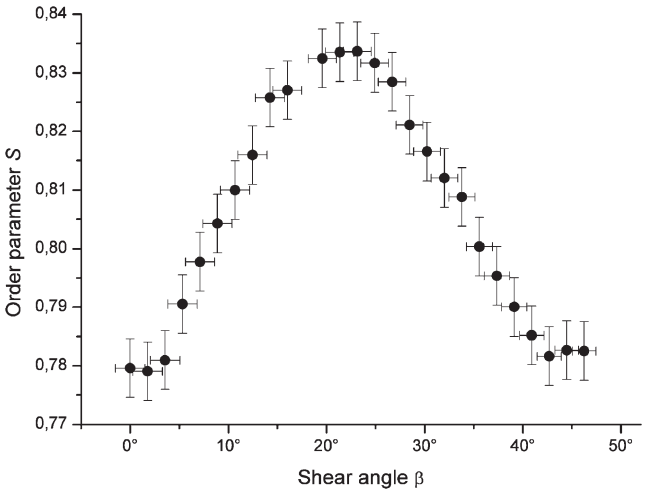


**Figure 7.** Order parameter $S$ as a function of shear at $T_{red} = 0.944$. After an initial increase, the order parameter starts to drop at shear angles above 30°. The apex coincides with the intrinsic SmC-tilt angle $\theta = 28°$.

the experimental data satisfactory (upper plot of Figure 5). A superposition of a pure Gaussian and a pure Lorentzian gives a far better result (lower plot of Figure 5) with a more narrow confidence interval of the fitting parameters. However, a pure Gaussian and pure Lorentzian is hypothetical and not based on any experimental evidence. We suspect that real underlying line shapes are two *pseudo*-Voigt functions of different $\mu$ and azimuthal peak maxima. As such, the fitting function is heavily overparametrized and does not yield reasonable results. The simplified fitting approaches at least allow for a reliable extraction of the azimuthal peak maxima. Using two *pseudo*-Voigt functions or using a pure Gaussian and pure Lorentzian yields almost identical values for the azimuthal peak positions, which differ only within ±1°. Since the superposition of the Gaussian and Lorentzian fits the data best, the azimuthal positions determined by this fitting function was used in further investigations.

The azimutal position of the trailing director $\mathbf{n}_-$ and the leading director $\mathbf{n}_+$ is shown in Figure 6. $\alpha = 0$ is set to be at the starting azimuthal position of the director. At low shear angles, only one director is present and $\mu$, which is the fraction of Lorentzian line shape in the wide-angle distribution, increases linearly with increasing shear angle $\beta$. At a shear angle of roughly $\beta \approx 23°$, $\mu$ reaches a maximum and starts to decline again. Presumably, the decline is a result of the start of the splitting process and the *pseudo*-Voigt function does not give reasonable results anymore. In the same regime, between a shear angle of 23° and 28°, the splitting is observed in the multiple-peak function. In the regime of the splitting, the angular position of the director that was obtained by fitting the data assuming only one peak respectively, and the superposition of two peaks overlap reasonably. The splitting into two directors takes place in the vicinity of the intrinsic smectic tilt angle $\theta = 28°$ that was found in the nonsheared samples (see Table 3).

The director rotates faster than the imposed shear before the splitting process at a slope of $\alpha = 1.4\beta$ After the splitting process, the leading director $\mathbf{n}_+$ undergoes a steep rise and at high shears it rotates nearly affine $\alpha_+ = \alpha_0 + 1.0\beta$, where $\alpha_0$ is the axis intercept. The trailing director $\mathbf{n}_-$ levels out and reaches a plateau of roughly $\alpha_- \approx 35°$. This means that the trailing director $\mathbf{n}_-$ is fixed at an inclination of roughly 35° with respect to the $z$-axis. With the initial

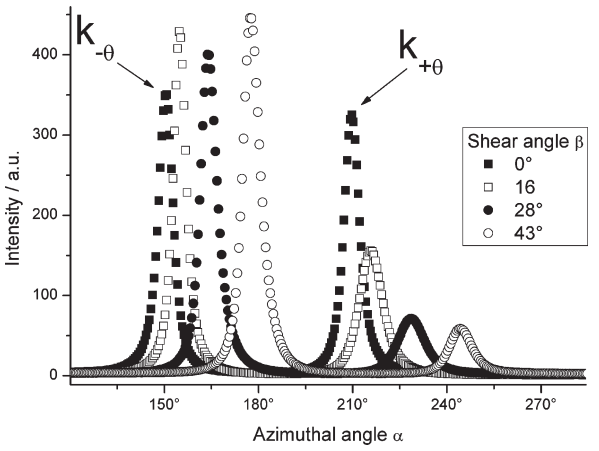


**Figure 8.** Azimuthal X-ray intensity distribution of **E7** in the small angle region for several shear angles at $T_{red} = 0.944$.

smectic tilt angle found to be $\theta = 28°$, one could assume that the smectic layer normal $\mathbf{k}_{-\theta}$ is aligned perpendicular to the $x$-axis. Analysis of the small-angle regime, however, shows that this is not the case. This will be discussed in the following section.

With the split-up of the wide-angle peak into two separate peaks, the calculation of the order parameter according to the model of Mitchell, Lovell, and Windle[29,30] is no longer valid. However, at shear angles $\beta < \theta$, little or no splitting was observed and the order parameter can be calculated accordingly by evaluation of the azimuthal intensity distribution in the wide-angle regime.[29,30] Figure 7 shows the order parameter of the sample as a function of the shear angle. After an initial rise, the order parameter starts to drop again, with the maximum being in the range of 20−25° of shear, which again coincides with the intrinsic smectic tilt angle $\theta$ . At higher shears, as the splitting of the directors takes place, the order parameter begins to drop. In previous studies this rise in order parameter was reported, but not the decline at shear angles above the intrinsic smectic tilt angle.[24] This behavior of the order parameter can be explained by the fact that the order parameter $S$ as observed by X-ray scattering, can be described by

$$S = S_n S_d \tag{2}$$

where $S_n$ is the nematic order parameter and $S_d$ is the domain order parameter. Any liquid crystal elastomer consists of individual domains with the nematic order parameter $S_n$. When stretching a elastomer uniaxially, the mechanical field couples to the domain order parameter $S_d$ and aligns the domains macroscopically. In a liquid single crystal elastomer, $S_d \approx 1$ and thus $S \approx S_n$. The nematic order parameter $S_n$ is mainly dependent on the temperature but hardly dependent on external mechanical fields.[2] Consequently, also the shear field will only couple to $S_d$ and we assume that $S_n \sim const$. Therefore, the significant change of S is a result of an alignment of the domains. Thus, at zero shear where $S = 0.78$ the domains are not oriented completely and $S_d < 1$. With increasing shear, the domains align and $S_d \approx 1$ at the maximum. At higher shear angles, two directors are formed, the alignment breaks down and the domain order parameter decreases, $S_d < 1$.

It would be desirable to subtract either the Lorentzian or the Gaussian fraction from the scattering data (see Figure 5). Then the order parameter could be calculated separately for both populations. However, subtraction of either of the

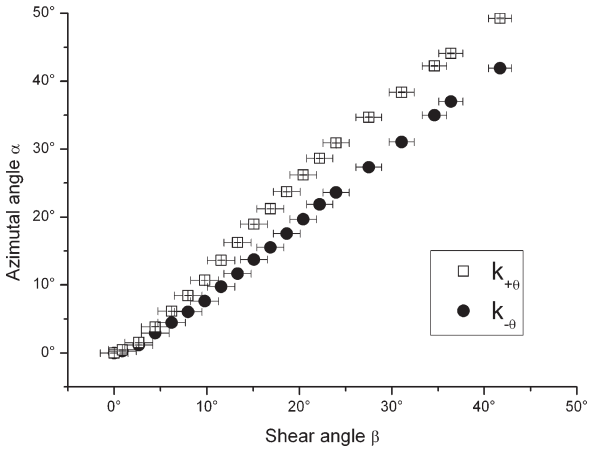


**Figure 9.** Azimutal position α of the SAXS-peaks as a function of the shear angle $\beta$ at $T_{red} = 0.944$.

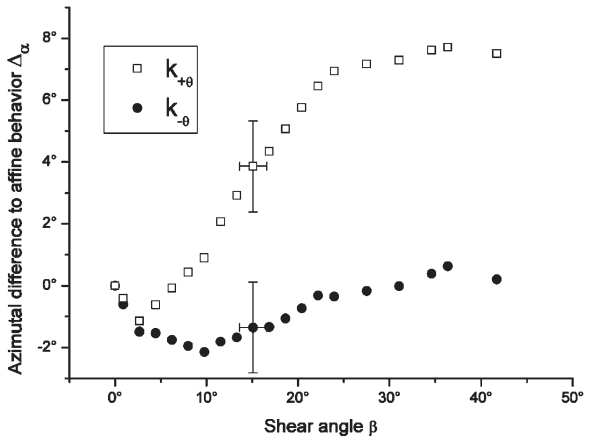


**Figure 10.** Difference to completely affine behavior of the SAXS-peaks as a function of the shear angle ($T_{red} = 0.944$).

peaks from the scattering data yields highly erratic line shapes which does not allow calculation of the order parameter. This is another hint that the result of the fitting process with the multiple-peak function is only valid to determine the azimuthal position of the two directors but must not be used for a line shape analysis.

**Small-Angle Regime.** To quantify the reorientation process of the smectic layers, synchrotron measurements of the small-angle regime were performed. Figure 8 shows the azimutal intensity distribution at angles of 0, 16, 28 and 43° of shear. The fading of the peak $\mathbf{k}_{+\theta}$ and the rising of the peak $\mathbf{k}_{-\theta}$ is clearly visible.

The azimutal position and peak area of the small-angle peaks and thus the smectic layer normal $\mathbf{k}$ can be determined by nonlinear fitting of the azimuthal intensity distribution using a *pseudo*-Voigt linear combination. To obtain the best fit of the experimental intensity distribution, the linear combination parameter of the *pseudo*-Voigt fitting function constantly decreases from $\mu \approx 0.7 \pm 0.03$ to $\mu \approx 0.6 \pm 0.03$ for both peaks throughout the shear experiment.

Figure 9 shows the change of the azimutal position α of the layer normals $\mathbf{k}_{-\theta}$ and $\mathbf{k}_{+\theta}$. By definition, $\alpha = 0$ at the staring azimuthal position of each peak. Clearly, the two peaks are moving at different affinity with respect to the shear deformation. $\mathbf{k}_{-\theta}$ moves nearly affine with the slope $\approx 1 \pm 0.1$. $\mathbf{k}_{+\theta}$ rotates at a higher rate than the imposed shear: at a shear angle of $\beta = 42°$ the peak has rotated by $\alpha_{k+\theta} = 49°$, with a resulting slope of $\approx 1.3 \pm 0.1$.

In the wide-angle regime it was found that the trailing director $\mathbf{n}_-$ stays fixed at an inclination of roughly 35° with respect to the $z$-axis. Neither of the layers, however, show such behavior and both layer populations continue to rotate even at high shear angles. For some reason, the rotation of the director and the layers is not directly coupled. Note that the small nonlinear part at shear angles near zero is probably resulting from nonperfect clamping conditions of the elastomer. Great care was taken in order to orient the director along the $z$-direction but small deviations in the range of 2° may have occurred.

The difference Δα to purely affine behavior can be quantified by subtracting the theoretical completely affine deformation where $\alpha = \beta$ from the actual azimuthal position (Figure 10). At shear angles $\beta < 3°$, both peaks seem to fall behind the imposed shear and splitting is observed. The peak $\mathbf{k}_{-\theta}$ is constantly 0 to 2° behind the imposed shear and moves almost completely affine. The peak $\mathbf{k}_{+\theta}$ moves at a higher rate than the imposed shear and, at a shear angle of roughly

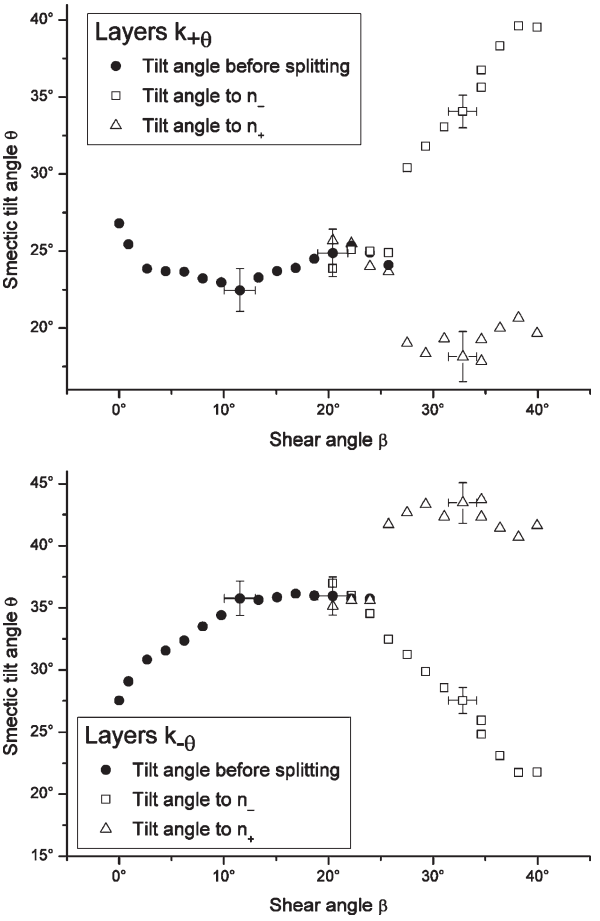


**Figure 11.** Smectic tilt angles as a function of shear as calculated from the director positions from Figure 6 for layer normals $\mathbf{k}_{-\theta}$ and $\mathbf{k}_{+\theta}$ at $T_{red} = 0.944$.

$\beta \approx 25°$, a plateau of $\Delta\alpha_{\mathbf{k}+\theta} \approx 8°$ is reached. As discussed in the preceding paragraph, the dip in the curve at very low shear angles is probably due to nonperfect clamping conditions. We may assume that in a sample where the director is perfectly aligned along the $z$-axis, the splitting of the affinity would occur at the first shear step. Thus, as in the wide-angle regime, the system breaks up in two populations that move with different rotational affinity, namely the layers of $\mathbf{k}_{-\theta}$ and $\mathbf{k}_{+\theta}$. In contrast to the wide-angle regime, the breakup in two populations happens at very low shears of

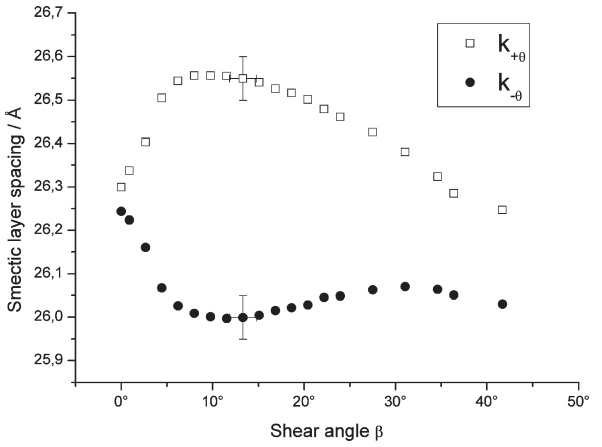


**Figure 12.** Layer spacing $d$ as a function of shear at $T_{red} = 0.944$.

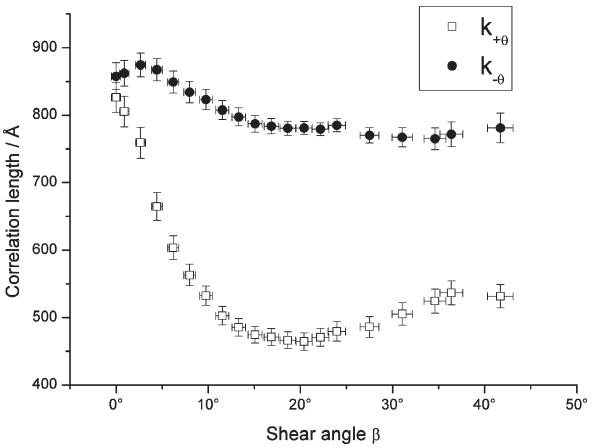


**Figure 13.** Correlation length $\zeta$ of the layers $\mathbf{k}_{-\theta}$ and $\mathbf{k}_{+\theta}$ as a function of shear at $T_{red} = 0.944$.

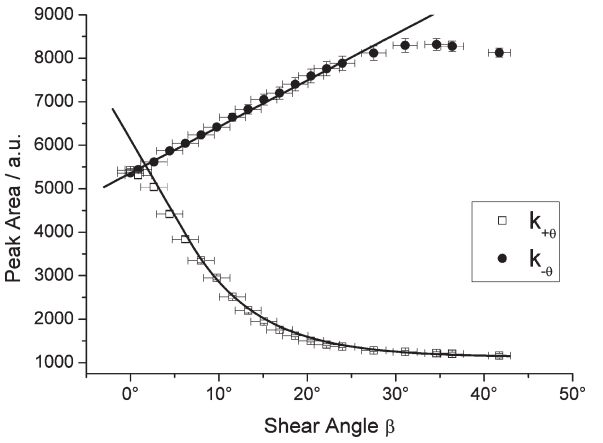


**Figure 14.** Area of the SAXS-peaks upon shear at $T_{red} = 0.944$.

around $\beta \approx 5°$. However, a process is also observed at a shear angle equal to the intrinsic smectic shear angle ($\beta \approx \theta = 28°$), where $\mathbf{k}_{+\theta}$ shows a distinct change of the slope of the affinity difference $\Delta\alpha$.

The smectic tilt-angle $\theta$, which is the angular difference between the orientation of the smectic layer normal **k** and the director **n**, can be calculated from the azimutal position of the wide-angle peak and the azimutal position of the small-angle peak. Since the smectic layers $\mathbf{k}_{-\theta}$ move with a different affinity than the layers $\mathbf{k}_{+\theta}$ two tilt-angles have to be calculated. For low shear angles the two tilt angles can be calculated accordingly. For high shears, however, a splitting of the sample in two director populations was proposed. Thus, $2 \times 2$ tilt angles have to be considered.

Figure 11 shows the calculated tilt angles. The tilt angle of $\mathbf{k}_{-\theta}$ (upper plot in Figure 11) shows a sharp rise at low shear angles and then levels out into a plateau where $\theta \approx 37°$. In the regime of the director splitting, the tilt angle relative to the leading director $\mathbf{n}_+$ shows another sharp rise and then reaches a plateau at $\theta \approx 44°$. The tilt angle relative to the trailing director $\mathbf{n}_-$ decreases in an almost linear fashion after the splitting regime. The tilt angle of $\mathbf{k}_{+\theta}$ undergoes a small drop in $\theta$ at small shear angles and reaches a plateau of roughly $\theta \approx 24°$. After splitting, the tilt angle shows similar behavior as in the case of the other small angle peak. The tilt angle relative to the trailing director $\mathbf{n}_-$ shows a linear increase, while the other tilt angle (relative to the leading director $\mathbf{n}_+$) approaches a plateau of roughly $\theta \approx 20°$.

The linear dependence of the tilt angle $\theta$ relative to the trailing director is found for both layer populations. This can be explained by the behavior of the trailing director which was found to be almost stationary at high shear angles (Figure 6). Both layer populations continue to rotate after the directors have split and thus seem to be decoupled from the trailing director $\mathbf{n}_-$. Because both layer populations seem to exhibit almost constant tilt angles relative to the leading director, it seems that both $\mathbf{k}_{+\theta}$ and $\mathbf{k}_{-\theta}$ solely follow the rotation of the leading director $\mathbf{n}_+$, albeit at different tilt angles.

According to eq 1, a change in the smectic tilt angle $\theta$ should also result in a change of the layer spacing $d$ and *vice versa*. Calculation of the expected change in the smectic layer spacing by using the tilt angles shown in Figure 11, a rise in the range of 1.8 Å ± 0.2 Å is expected for the layers in the $\mathbf{k}_{+\theta}$ at shear angles before the director splitting takes place. For the layers $\mathbf{k}_{-\theta}$, a shrinkage in the range of 1.6 Å ± 0.2 Å is expected in the same regime.

Figure 12 shows the experimentally determined smectic layer spacing as a function of the shear angle $\beta$ . Both layer populations show an initial value of $d = 26.3$ Å. The layers $\mathbf{k}_{-\theta}$ seem to shrink slightly upon shear and then, at shear values $\beta$ larger than the initial smectic tilt angle, the layer spacing seems to reach a plateau of roughly 25 to 26 Å. The layers $\mathbf{k}_{-\theta}$ expand up to values of 26.6 Å and then start to decrease linearly. At a shear angle of $\beta = 42°$, the layers have once more reached the initial spacing of $d = 26.3$ Å.

The change of layer spacing found here is in the range of about 0.3 ± 0.2 Å and thus far below the change of layer spacing expected from the calculations using the smectic tilt angle according to eq 1. Similar to what was found in the comparison of the directors' and the layer normals' azimuthal rotation, the layer spacing seems to be independent of the tilt angle.

From the radial full width at half-maximum (fwhm) of the small-angle peaks, the correlation length $\zeta$ of the smectic layers can be calculated by $\zeta = 2^* \pi/\text{fwhm}$. The shear-angle dependent values of $\zeta$ are plotted in Figure 13. In the unsheared state, all layers show the same correlation length of about $\zeta = 850$ Å ± 25 Å. Other reports on main-chain systems find correlation lengths in the range of $\zeta = 1200$ Å.[34] The correlation length found here is in the same order of magnitude. Upon shear, the layers $\mathbf{k}_{-\theta}$ show only a small decrease in the correlation length until reaching a plateau of $\zeta = 800$ Å. The layers $\mathbf{k}_{+\theta}$ however, show a steep drop in the correlation length with a minimum of $\zeta = 450$ at 20° of shear angle. For high shears the correlation length of $\mathbf{k}_{+\theta}$ reaches a plateau at around $\zeta = 525$ Å.

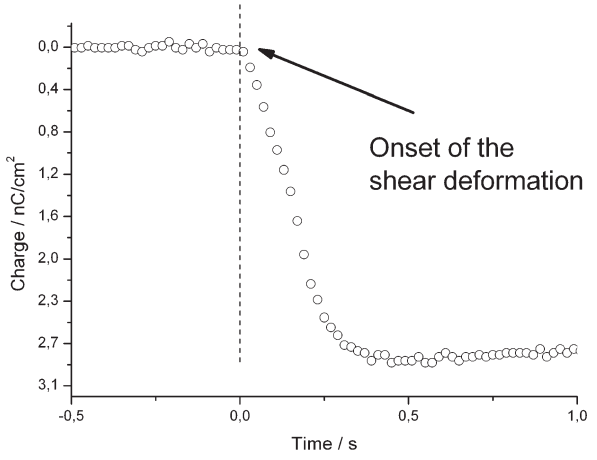


**Figure 15.** Charge formation of E11 when shearing from 6.5 to 9.0° at $T_{red} = 0.944$.

Figure 14 shows the peak area of both peaks. The peak $\mathbf{k}_{-\theta}$ grows linearly with increasing shear. The linear regimes end at a shear angle of $\beta \approx 25°$ and the peak area reaches a limit of roughly double the value at $\beta = 30°$.The other peak, $\mathbf{k}_{-\theta}$, decreases exponentially and approaches a limit of roughly a fifth of its initial value. The exponential decay does not start immediately at $\beta = 0$, which again might be a result of nonperfect clamping conditions. Also in this plot, we find a split in two populations of layers that behave completely different. Similar to the previous results, a distinct change is found at shear angles of $\beta \approx 25°$, which coincides with the intrinsic smectic tilt angle $\theta$ at zero shear.

Previous reports[24,25] interpreted this growth of the peak $\mathbf{k}_{-\theta}$ to be the result of a transformation process, where the layers $\mathbf{k}_{+\theta}$ are gradually aligned with the layers $\mathbf{k}_{-\theta}$. With the two different growth rates of the two peaks found here, this process seems unlikely. A possible explanation is given by a model developed by James Adams and Mark Warner,[23] where they describe the shear induced reorientation process of a SmC-LCE. If we consider that at zero shear the smectic layer normals are distributed conically around the director which points along the $z$-axis of our experiment, then only a small fraction of the layer normals is aligned parallel to the $x-z$-plane. Only this fraction is contributing to the scattering process. The larger part of the smectic layer normals are pointing at directions not parallel to the $x-z$-plane. Analog to the layers that are detected in the scattering experiment, the layers with their normals outside the $x-z$-plane can be divided into two populations: $\mathbf{k}_{-\theta}$ in the hemisphere at the negative part of the $x$-axis and $\mathbf{k}_{-\theta}$ in the hemisphere at the positive part of the $x$-axis (Figure 4).

Upon shear, all the layers $\mathbf{k}_{-\theta}$ will migrate to align their layer normal parallel to the $x-z$-plane, causing a distinct rise in the scattering intensity. When the shear angle $\beta$ approaches the intrinsic smectic tilt angle $\theta$, the most favorable state for these layers has been reached. In contrast, the layer normals $\mathbf{k}_{+\theta}$ will migrate out of the $x-z$-plane which can be seen by a decrease in the scattering intensity. This migration process which leads to an disordered state is supposedly also the reason for the low smectic correlation of $\mathbf{k}_{+\theta}$ However, not all layer normals $\mathbf{k}_{+\theta}$ leave the direction parallel to the $x-z$-plane, which is also in agreement with the theoretical model. The model even predicts that at very high shear angles, the peak $\mathbf{k}_{+\theta}$ should increase again, as the layer normals will realign parallel to the $x-z$-plane. Such behavior is not found at the shear angles that we can reach in our experiments.

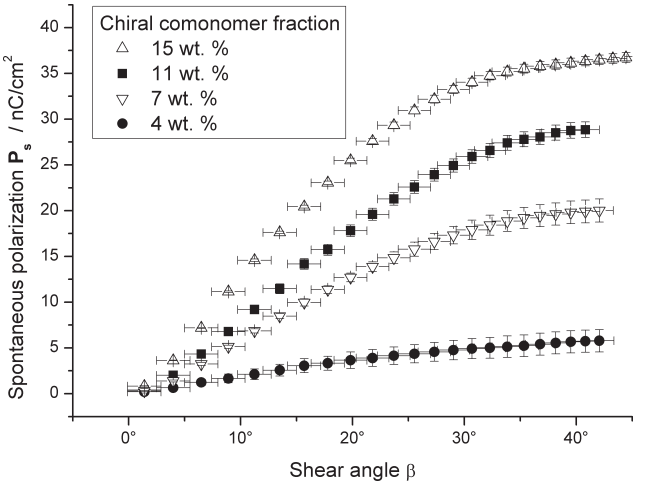


**Figure 16.** Charge formation when the LCE were subjected to simple shear at $T_{red} = 0.944$. The occurring charge depends on the amount of chiral dopant content and is highest in the LCE **E15** with 15 wt % of chiral compound.

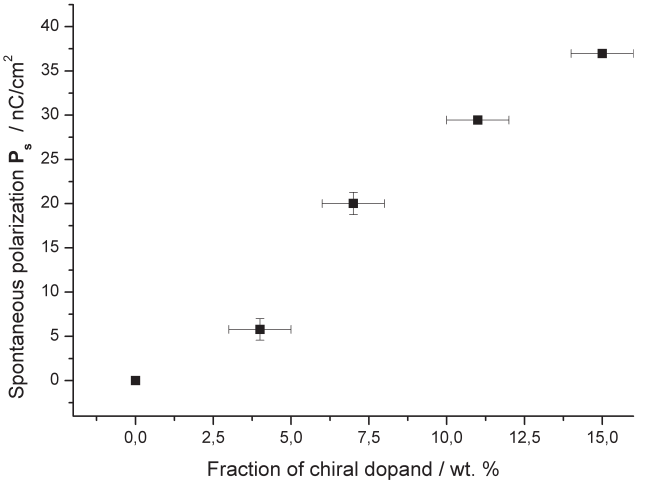


**Figure 17.** Dependence of the spontaneous polarization $\mathbf{P_s}$ on the chiral dopant concentration at $T_{red} = 0.944$.

**Spontaneous Polarization.** The reorientation process of the smectic layers leads to a macroscopic alignment of the electric polarization vectors of the SmC*-phase along the $y$-axis of the experiment. As a result, charges are formed on the surface of the sample. To investigate this alignment process, shear experiments were conducted for all elastomers. The shear setup was the same as in the X-ray experiments. Additionally, silver conductive paste was spread on the film on both sides to allow for electric contacting.

A typical response of the sample when deformed by a simple shear is shown in Figure 15. The sample **E11** doped with 11 wt % was sheared from $\beta = 6.5$ to $\beta = 9.0°$. A resulting charge of $2.8 \pm 0.1$ nC/cm$^2$ is formed in this shear interval. The charge formation begins at the same moment as the shear deformation starts. No further charge formation was detected after the shear step was stopped. Please note that the rise in charge after the deformation is not due to relaxation of the sample but is an artifact resulting from the signal drift of the used charge amplifier.

Figure 16 shows the spontaneous polarization $\mathbf{P_s}$ of all elastomers as a function of the shear angle. The $\mathbf{P_s}$ rises with increasing content of chiral compound. At small shear angles, the spontaneous polarization is linearly dependent

on the shear angle. There is a distinct change of the slope at $\beta = 25-30°$ for all elastomers, close to the intrinsic smectic tilt-angle $\theta$. When comparing this result to the shear-angle dependence of the smectic layer structure (see Figure 14), we find that the maximum formation of charges takes place in the regime where the layers $\mathbf{k}_{-\theta}$ are entering the $x-z$-plane. At shear angles above $\beta = 30°$, where the smectic layers $\mathbf{k}_{-\theta}$ have stopped migrating into the $x-z$-plane, $\mathbf{P_s}$ hardly changes. However, charges are formed even at high shear angles. This is most likely because of the migration of the layers $\mathbf{k}_{+\theta}$ (whose vector of spontaneous polarization opposes that of $\mathbf{k}_{-\theta}$) out of the $x-z$-plane.

The spontaneous polarization $\mathbf{P_s}$ of all elastomers as a function of the chiral dopant fraction is shown in Figure 17. Clearly, the $\mathbf{P_s}$ rises with increasing amounts of chiral dopant in a linear fashion. Comparison of the $\mathbf{P_s}$-values found here with the results published by Chan et al.[28] for a structurally similar low molar mass system, reveals that the spontaneous polarization in the systems at hand is lower by a factor of 5. Chan found $\mathbf{P_s}$-values of 70−180 nC/cm$^2$ for a low molar mass liquid crystal doped with 10 wt % of several chiral dopants that were structurally similar to the one used in this work. We can only speculate as to why the values of $\mathbf{P_s}$ are lower in the investigated elastomers. With the results from the X-ray experiments of the shear process several explanations could be given. First of all, the mondomain formation of the smectic layers is not complete. Roughly 10% of the smectic layers $\mathbf{k}_{+\theta}$ remain, thus lowering the net polarization. However, this result obviously only accounts for a loss of about 10−20%.

On the other hand, the X-ray data and the theoretical model of Adams et al. suggests, that the layers $\mathbf{k}_{+\theta}$ do not realign with the layers $\mathbf{k}_{-\theta}$. Rather, these layers just leave the $x-z$-plane. Thus, the $\mathbf{P_s}$ measured is only the sum of the polarization of layers that have aligned in the $x-z$-plane, which should be half of the actual layers present in the sample. Taking these circumstances into account, a theoretical $\mathbf{P_s}$ of roughly 60 nC/cm$^2$ for the sample **E11** with 11 wt % of chiral dopant fraction can be calculated which is almost as high as the spontaneous polarization found in the systems of Chan et al.. Also, it should be considered that in their measurements Chan et al. used a host-system which was highly optimized to support high values of spontaneous polarization while the system used in our studies was not, which should also lead to lower values of $\mathbf{P_s}$.

## Conclusion

A series of SmC-elastomers with varying amount of chiral dopant were synthesized. All elastomers exhibit a smectic-C-phase. The phase transition temperature at which isotropization occurs is around 65 to 75 °C depending on the concentration of chiral dopant. With increasing amounts of chiral dopant, a decrease in the smectic tilt angle $\theta$ and a slight increase in the smectic layer spacing $d$ is found. The order parameter is not affected by the addition of chiral dopant. By exposure to shear deformation, macroscopic realignment of the smectic layers and thus the polarization vectors of the SmC*-phase is accomplished. The reorientation process was followed by shear-angle dependent X-ray diffraction and also by the measurement of charge formation on the elastomer's surface.

The X-ray measurements revealed that simple shear does not lead to complete macroscopic uniform layer orientation. Rather, at shear angles in the range of the intrinsic smectic tilt angle, the shear process causes a splitting of the wide-angle scattering distribution. We interpreted this observation in terms of a splitting in domains of two different director orientations. The leading director $\mathbf{n}_+$ moves faster than the shear angle, while the trailing director $\mathbf{n}_-$ seems to stay stationary at an inclination of roughly 35° with respect to the $z$-axis. The order parameter of the sample rises until the splitting into two directors takes place. The order parameter of the individual populations could not be determined because the line shape of the individual scattering distributions could not be determined precisely enough. For further investigations of the order parameter of the individual populations, a new description of the orientational distribution function, which incorporates the splitting of the director, has to be developed.

Independent of the shear angle, the orientational distribution of the smectic layer is found to be of Lorentzian line shape. The smectic layers $\mathbf{k}_{-\theta}$ move with a different affinity than the layers $\mathbf{k}_{+\theta}$. Unlike the trailing director, however, neither of the layers enter a stationary inclination. In the proposed model of a splitting of the director, the layers seem to be decoupled from the trailing director $\mathbf{n}_-$ and solely follow the leading director $\mathbf{n}_+$. The resulting change of the tilt angle should also result in a change of the smectic layer spacing. However, this change was not found in our experiments. At low shear angles, the layers $\mathbf{k}_{-\theta}$ migrate to the $x-z$-plane, which can be seen by a linear rise in the scattering intensity. When the shear angle reaches the intrinsic smectic tilt angle, this reorientation process is finished and the scattering intensity of these peaks stays constant. The layers $\mathbf{k}_{+\theta}$ simply leave the $x-z$-plane upon shear and do not realign with the layers $\mathbf{k}_{-\theta}$. This finding agrees well with the theoretical model developed by Adams et al.[23]

All doped elastomers are electromechanically active. The formation of charges on the elastomer's surface is highly dependent on the shear angle. The maximum charge formation takes place at shear angles where the smectic layers $\mathbf{k}_{-\theta}$ are entering the $x-z$-plane. Once this migration process stops at a shear angle close to the intrinsic tilt angle $\theta$, the spontaneous polarization stays almost constant. The spontaneous polarization in this homologous series is linearly dependent on the amount of chiral dopant. Values of $\mathbf{P_s}$ of up to 37 nC/cm$^2$ have been measured. This is lower than what has been reported for structurally similar low molar mass SmC* liquid crystals.[28] When considering the imperfect realignment process of the simple shear deformation, a theoretical spontaneous polarization of about 60 nC/cm$^2$ for a sample doped with 11 wt % of chiral dopant can be calculated. Other realignment methods where all smectic layers are aligned macroscopically will have to be employed in order to actually measure the real $\mathbf{P_s}$ of these systems.

**Acknowledgment.** The authors thank James Adams and Mark Warner for fruitful discussions and the Helmholtz Association for providing beam time at BW4 of the HASYLAB synchrotron facility in Hamburg, Germany. Funding by Nissan Motors Co. and Deutsche Forschungsgemeinschaft through SFB 428 is gratefully acknowledged.

## References and Notes

(1) Warner, M.; Terentjev, E. M. *Liquid Crystal Elastomers*, 2nd ed.; Oxford University Press: Oxford, U.K., 2007.
(2) Krause, S.; Zander, F.; Bergmann, G.; Brandt, H.; Wertmer, H.; Finkelmann, H. *C. R. Chim.* **2009**, *12*, 85–104.
(3) Mayer, S.; Zentel, R. *Curr. Opin. Solid. State Mol.* **2002**, *6*, 545–551.
(4) Bahr, C. In *Chirality in Liquid Crystals*; Kitzerow, H. S., Bahr, C., Eds.; Springer: New York, 2001.
(5) Hird, M.; Goodby, J. W.; Hindmarsh, P.; Lewis, R. A.; Toyne, K. J. *Ferroelectrics* **2002**, *276*, 219–237.
(6) Meyer, R. B.; Liebert, L.; Strzelecki, L.; Keller, P. *J. Phys. Lett.-Paris* **1975**, *36*, 69–71.
(7) Lehmann, W.; Gattinger, P.; Keck, M.; Kremer, F.; Stein, P.; Eckert, T.; Finkelmann, H. *Ferroelectrics* **1998**, *208*, 373–383.

(8) Eckert, T.; Finkelmann, H.; Keck, M.; Lehmann, W.; Kremer, F. *Macromol. Rapid Commun.* **1996**, *17*, 767–773.
(9) Benne, I.; Semmler, K.; Finkelmann, H. *Macromolecules* **1995**, *28*, 1854–1858.
(10) Benne, I.; Semmler, K.; Finkelmann, H. *Macromol. Rapid Commun.* **1994**, *15*, 295–302.
(11) Spillmann, C. M.; Ratna, B. R.; Naciri, J. *Appl. Phys. Lett.* **2007**, *90*, 021911.
(12) Walba, D. M.; Yang, H.; Shoemaker, R. K.; Keller, P.; Shao, R. F.; Coleman, D. A.; Jones, C. D.; Nakata, M.; Clark, N. A. *Chem. Mater.* **2006**, *18*, 4576–4584.
(13) Brand, H. R.; Cladis, P. E.; Finn, P. L. *Phys. Rev. A* **1985**, *31*, 361–365.
(14) Lagerwall, J. P. F.; Giesselmann, F. *ChemPhysChem* **2006**, *7*, 20–45.
(15) Haseloh, S.; Zentel, R. *Macromol. Chem. Phys.* **2009**, *210*, 1394–1401.
(16) Komp, A.; Rühe, J.; Finkelmann, H. *Macromol. Rapid Commun.* **2005**, *26*, 813–818.
(17) Küpfer, J.; Finkelmann, H. *Makromol. Chem. Rapid Commun.* **1991**, *12*, 717–726.
(18) Nishikawa, E.; Finkelmann, H.; Brand, H. R. *Macromol. Rapid Commun.* **1997**, *18*, 65–71.
(19) Nishikawa, E.; Finkelmann, H. *Macromol. Chem. Phys.* **1997**, *198*, 2531–2549.
(20) Komp, A.; Finkelmann, H. *Macromol. Rapid Commun.* **2007**, *28*, 55–62.
(21) Kramer, D.; Finkelmann, H. *Macromol. Rapid Commun.* **2007**, *28*, 2318–2324.
(22) Stein, P.; Finkelmann, H. In *Chirality in Liquid Crystals*; Kitzerow, H. S., Bahr, C., Eds.; Springer: New York, 2001.
(23) Adams, J. M.; Warner, M. *Phys. Rev. E* **2008**, *77*, 021702.
(24) Sanchez-Ferrer, A.; Finkelmann, H. *Macromolecules* **2008**, *41*, 970–980.
(25) Hiraoka, K.; Finkelmann, H. *Macromol. Rapid Commun.* **2001**, *22*, 456–460.
(26) Marcus, J.; Brussee, J.; van der Gen, A. *Eur. J. Org. Chem.* **1998**, 2513–2517.
(27) Donnio, B.; Wermter, H.; Finkelmann, H. *Macromolecules* **2000**, *33*, 7724–7729.
(28) Chan, L. K. M.; Gray, G. W.; Lacey, D.; Scrowston, R. M.; Shenouda, I. G.; Toyne, K. J. *Mol. Cryst. Liq. Cryst.* **1989**, *172*, 125–146.
(29) Mitchell, G. R.; Lovell, R. *Acta Crystallogr A* **1981**, *37*, 189–196.
(30) Mitchell, G. R.; A.H., W. In *Developments in Crystalline Polymers*; Basset, D. C., Ed.; Elsevier Applied Science: New York, 1988; pp 115−175.
(31) Hiraoka, K.; Nose, T.; Uematsu, Y.; Tokita, M.; Watanabe, J. *Liq. Cryst.* **2007**, *34*, 305–310.
(32) Beyer, P.; Terentjev, E. M.; Zentel, R. *Macromol. Rapid Commun.* **2007**, *28*, 1485–1490.
(33) Lagerwall, J. P. F.; Giesselmann, F.; Radcliffe, M. D. *Phys. Rev. E* **2002**, *66*, 031703.
(34) de Jeu, W. H.; Obraztsov, E. P.; Ostrovskii, B. I.; Ren, W.; McMullan, P. J.; Griffin, A. C.; Sanchez-Ferrer, A.; Finkelmann, H. *Eur. Phys. J. E* **2007**, *24*, 399–409.